

# On the Relationship Between Representation Geometry and Generalization in Deep Neural Networks

Sumit Yadav <sup>1</sup>

<sup>1</sup>Institute of Engineering, Pulchowk Campus, Tribhuvan University, Nepal

*076bct088.sumit@pcampus.edu.np*

**Abstract.** Understanding the factors that determine neural network generalization remains a fundamental challenge in deep learning theory. We investigate the relationship between the geometry of learned representations and model performance through systematic empirical studies spanning vision and language domains. Analyzing 52 pretrained ImageNet classifiers across 13 architecture families, we demonstrate that effective dimension—an unsupervised geometric metric requiring no labels—strongly predicts classification accuracy. **Output effective dimension** shows the strongest partial correlation with accuracy (partial  $r = 0.75$ ,  $p < 10^{-10}$ ) after controlling for model capacity, while **total compression**—the log-ratio of output to input effective dimensionality—achieves  $r = -0.65$  (partial  $r = -0.72$ ). These dual geometric signatures form a complementary framework: output effective dimension captures representation richness while compression captures information refinement. Our findings replicate across in-distribution (ImageNet) and transfer (CIFAR-10) settings. We demonstrate cross-domain generalization: effective dimension metrics predict performance for 8 encoder models on NLP tasks (SST-2, MNLI) and 15 decoder-only LLMs (GPT-2, OPT, Qwen, SmollM, Phi) on AG News, where compression correlates with representation quality ( $r = 0.69$ ,  $p = 0.004$ ) while model size does not ( $r = 0.07$ ). We establish **bidirectional causality through controlled intervention**: degrading geometry via noise injection causes accuracy loss ( $r = -0.94$ ,  $p < 10^{-9}$ ), while improving geometry via PCA projection maintains accuracy across multiple architectures (mean  $-0.03$ pp loss at 95% variance across ResNet18, ResNet34, DenseNet121). Critically, this relationship is **noise-type agnostic**: Gaussian ( $r = -0.94$ ), Uniform ( $r = -0.96$ ), Dropout ( $r = -0.91$ ), and Salt-and-pepper ( $r = -0.99$ ) noise all show strong negative correlations. These results establish that effective dimension geometry—computed entirely without labels—provides domain-agnostic predictive and causal information about neural network performance.

**Keywords:** *representation learning · generalization · effective dimension · neural networks · information geometry*

## 1 Introduction

A central question in deep learning theory is: *what properties of learned representations enable generalization?* While architectural innovations, from ResNets [1] to EfficientNets [2], Vision Transformers [3], and modern hybrids like ConvNeXt [4] and Swin [5], have driven substantial empirical progress, theoretical understanding of why certain networks generalize better than others remains incomplete. Classical generalization bounds based on VC dimension or Rademacher complexity are often vacuous for overparameterized networks [6], [7], motivating the search for alternative characterizations. Indeed, Zhang et al. [8] demonstrated that networks can memorize random labels yet still generalize on real data, fundamentally challenging classical theory.

Recent work suggests that neural network representations may be converging toward universal geometric structures. The Platonic Representation Hypothesis [9] proposes that diverse AI models are converging toward a shared statistical model of reality, with vision and language models increasingly measuring distances between datapoints in similar ways as they scale. This convergence implies that geometric properties of representations may be fundamental rather than architecture-specific, motivating our investigation of whether geometric signatures predict performance across diverse architectures and domains.

The information bottleneck (IB) principle [10], [11] posits that optimal representations compress input information while preserving task-relevant features. This suggests examining the *geometry* of representations — their intrinsic dimensionality, clustering structure, and transformation properties — as potential indicators of generalization capability. Prior work has shown that intrinsic dimension correlates with accuracy [12] and that representations converge to structured configurations during training [13].

In this work, we conduct a systematic empirical investigation of the relationship between representation geometry and model performance. Our contributions are:

1. We introduce **total compression**  $\mathcal{C}$ , defined as the log-ratio of output to input effective dimensionality, as a unified geometric signature capturing the network’s information processing.
2. Through analysis of 52 pretrained models across 13 architecture families, we establish that total compression strongly predicts accuracy ( $r = -0.65$ ), with this relationship **strengthening** after controlling for model size (partial  $r = -0.71$ ).

3. We demonstrate **cross-distribution robustness**: geometric relationships hold on both native ImageNet and transferred CIFAR-10 evaluations, suggesting these properties reflect fundamental representation characteristics.
4. We show that **output effective dimension** is the strongest individual predictor of accuracy (partial  $r = 0.75$ ), stronger than total compression, demonstrating that networks maintaining higher effective dimensionality in final representations achieve better performance.
5. We demonstrate **cross-domain generalization**: effective dimension metrics predict performance for 8 encoder models (BERT, RoBERTa, ELECTRA, DistilBERT) on SST-2 and MNLI, and for 15 decoder-only LLMs (GPT-2, OPT, Qwen, SmolLM, Phi) on AG News. Compression correlates with representation quality ( $r = 0.69$ ) while model size does not ( $r = 0.07$ )—establishing that geometric signatures predict performance across architectures, tasks, and domains.
6. We establish **bidirectional causality through controlled intervention**: degrading geometry via noise causes accuracy loss ( $r = -0.94$ ,  $p < 10^{-9}$ ), while improving geometry via PCA maintains accuracy across three architectures (mean  $-0.03\text{pp}$  at 95% variance). This relationship is **noise-type agnostic**—all four tested noise types (Gaussian, Uniform, Dropout, Salt-and-pepper) show  $|r| > 0.90$ —demonstrating the geometry-performance relationship is causal and robust.

## 2 Related Work

**Information-Theoretic Perspectives.** The information bottleneck framework [10] characterizes learning as optimizing the trade-off  $\mathcal{L} = I(X; T) - \beta I(T; Y)$  between compression  $I(X; T)$  and prediction  $I(T; Y)$ . Shwartz-Ziv and Tishby [11] empirically observed distinct fitting and compression phases during training. However, Saxe et al. [14] demonstrated that compression behavior depends on activation functions and questioned whether IB explains generalization. Our approach sidesteps mutual information estimation difficulties by directly measuring geometric proxies.

**Representation Convergence.** Recent work suggests neural representations are converging across architectures and modalities. Huh et al. [9] demonstrate that vision and language models increasingly measure distances between datapoints in similar ways as they scale, hypothesizing convergence toward a “platonic representation”—a shared statistical model of reality. Jha et al. [15] demonstrate that embeddings can be translated across model families without paired data by learning a shared latent representation, providing direct evidence that geometric structure is preserved across architectures; their finding that translated embeddings retain sufficient semantics for attribute inference suggests that geometric signatures capture fundamental properties of representations. Noroozizadeh et al. [16] identify “geometric memory” in transformers, where models synthesize embeddings encoding global relationships rather than brute-force lookup. These findings suggest our geometric signatures may capture fundamental properties shared across architectures, explaining our cross-domain results.

**Representation Geometry.** Ansuini et al. [12] showed that intrinsic dimensionality follows an expansion-then-compression pattern across layers, with final-layer dimension predicting accuracy. Related work on intrinsic dimension [17], [18] provides tools for measuring representation complexity. SVCCA [19], CKA [20], and related methods [21], [22] enable representation comparison across networks. Neural collapse [13] describes the terminal training phase where class representations converge to a simplex equiangular tight frame. Transfer learning studies [23] demonstrate that learned features vary in transferability across layers. Olah [24] provided early intuitions connecting neural network layers to topological transformations, showing that classification requires sufficient dimensionality to untangle class manifolds. Zhang et al. [25] established connections between ReLU networks and tropical geometry, while Guss and Salakhutdinov [26] used algebraic topology to characterize network capacity. Our work extends these by systematically relating geometric properties to performance across architectures.

**Generalization Theory.** Classical bounds via VC dimension or Rademacher complexity scale with model capacity, yielding vacuous results for modern networks [7], [8]. Recent work connects generalization to flatness of loss landscapes [27], [28], [29], [30], dynamical isometry and singular value distributions [31], compression-based bounds [32], and the double descent phenomenon [33], [34]. The neural tangent kernel framework [35] provides theoretical grounding for infinite-width networks. Information geometry [36] offers a rigorous framework for studying statistical manifolds. Our geometric metrics provide empirically tractable correlates of these theoretical quantities [37].

## 3 Problem Formulation

### 3.1 Setup and Notation

Consider a neural network  $f_\theta : \mathcal{X} \rightarrow \mathcal{Y}$  parameterized by  $\theta \in \Theta$  trained on dataset  $\mathcal{D} = \{(x_i, y_i)\}_{i=1}^n$  for  $K$ -class classification. Let  $f_\theta$  be decomposed as  $f_\theta = g \circ h$  where  $h : \mathcal{X} \rightarrow \mathcal{Z}$  maps inputs to representations and  $g : \mathcal{Z} \rightarrow \mathcal{Y}$  is the classifier head.

For a set of inputs  $\{x_i\}_{i=1}^m$ , let  $\mathbf{Z} = [h(x_1), \dots, h(x_m)]^\top \in \mathbb{R}^{m \times d}$  denote the representation matrix. We analyze the geometry of  $\mathbf{Z}$  through the lens of effective dimensionality and class structure.

### 3.2 Effective Dimensionality

**Definition 1** (Effective Dimension). For representation matrix  $\mathbf{Z} \in \mathbb{R}^{m \times d}$  with centered covariance  $\Sigma = \frac{1}{m-1} \tilde{\mathbf{Z}}^\top \tilde{\mathbf{Z}}$  and eigenvalues  $\lambda_1 \geq \dots \geq \lambda_d \geq 0$ , the *effective dimension* is:

$$\text{EffDim}(\mathbf{Z}) = \frac{\left(\sum_{i=1}^d \lambda_i\right)^2}{\sum_{i=1}^d \lambda_i^2} = \frac{\text{tr}(\Sigma)^2}{\text{tr}(\Sigma^2)} \quad (1)$$

The effective dimension, also known as the participation ratio [12], quantifies the number of dimensions contributing meaningfully to variance. It equals  $d$  when variance is uniform across dimensions and approaches 1 when concentrated in a single direction. Unlike rank, it is continuous and robust to small eigenvalues. This measure is related to intrinsic dimension estimators used in representation analysis [12], [18].

### 3.3 Total Compression

For a network with  $L$  layers producing representations  $\mathbf{Z}^{(1)}, \dots, \mathbf{Z}^{(L)}$ , we define:

**Definition 2** (Total Compression). The *total compression* of network  $f_\theta$  is:

$$\mathcal{C}(f_\theta) = \log \left( \frac{\text{EffDim}(\mathbf{Z}^{(L)})}{\text{EffDim}(\mathbf{Z}^{(1)})} \right) \quad (2)$$

Negative values indicate the network reduces effective dimensionality (compresses), while positive values indicate expansion.

**Motivation for log-ratio.** We use the log-ratio rather than alternatives (e.g., difference  $d_L - d_1$  or sum of per-layer changes) for three reasons: (1) **Scale invariance**: the log-ratio is dimensionless, enabling comparison across architectures with different hidden dimensions; (2) **Multiplicative interpretation**: information processing across layers is compositional—the log converts multiplicative effects to additive; (3) **Comparability**: a network that compresses from 100→10 and one that compresses from 1000→100 both have  $\mathcal{C} = -2.3$ , reflecting equivalent relative transformation despite different absolute scales. This metric captures the network’s overall geometric transformation independent of absolute dimensions.

### 3.4 Output Effective Dimension

While total compression captures the overall transformation, the **output effective dimension**  $\text{EffDim}(\mathbf{Z}^{(L)})$  measures the richness of the final representation before classification. This single metric proves to be the strongest predictor of accuracy after controlling for model size, as networks that maintain higher effective dimensionality in their final layer tend to achieve better performance.

### 3.5 Theoretical Connections (Informal)

While our primary contribution is empirical, we note several **informal** connections between effective dimension and established theoretical frameworks. These are intended as motivation and intuition, not formal claims.

**Intuition from Rademacher Complexity.** For linear classifiers over a representation with effective dimension  $d_{\text{eff}}$ , standard bounds suggest Rademacher complexity scales roughly as  $\mathcal{O}\left(\sqrt{\frac{d_{\text{eff}}}{m}}\right)$  [38]. This provides intuition (though not a formal proof) for why lower effective dimension in final layers might relate to better generalization for downstream linear probes.

**Intuition from Fisher Information.** Under certain assumptions, effective dimension relates informally to the Fisher information matrix  $\mathbf{F}$  via the ratio  $\frac{\text{tr}(\mathbf{F})}{\|\mathbf{F}\|_{\text{op}}}$ . This suggests a conceptual connection to natural gradient geometry [39] and loss landscape curvature [27], though we do not claim a formal equivalence.

**Intuition from Intrinsic Dimension.** The participation ratio is related to intrinsic dimension estimators used in representation analysis [12], [18]. Networks that achieve lower effective dimension may be learning representations on lower-dimensional manifolds, consistent with the manifold hypothesis [40].

**Caveat.** These connections are suggestive, not rigorous. The precise relationship between effective dimension and generalization remains an open theoretical question. Our contribution is empirical: we demonstrate strong correlations and causal relationships between effective dimension and accuracy, but do not claim to have proven *why* this relationship holds. The empirical findings stand independent of any specific theoretical interpretation.

## 4 Methods

### 4.1 Experimental Design

**Pretrained Model Analysis.** We analyze 52 ImageNet [41] pretrained models from torchvision spanning 13 architecture families (Table 11): ResNet [1], Wide ResNet [42], ResNeXt [43], VGG [44], DenseNet [45], EfficientNet [2], EfficientNetV2 [46], MobileNet [47], [48], ShuffleNet [49], SqueezeNet [50], ConvNeXt [4], ViT [3], and Swin [5]. Models range from 1.2M to 306M parameters with top-1 accuracy from 58.1% to 85.8%.

**Datasets.** We evaluate geometry on: (i) **ImageNet-50k**: 50,000 images from ImageNet validation set at native  $224 \times 224$  resolution; (ii) **CIFAR-10 (transfer)**: 10,000 test images resized to  $224 \times 224$ , representing out-of-distribution transfer.

**Training-Time Analysis.** To study geometry evolution, we train 11 models from scratch on CIFAR-10 [51] for 50 epochs, spanning 6 architecture families: ResNet [1], MobileNet [47], [48], EfficientNet [2], VGG [44], DenseNet [45], and ShuffleNet [49]. Training uses SGD with momentum, batch normalization [52], and standard data augmentation. Checkpoints are saved at epochs  $\{1, 5, 10, 15, 20, 30, 40, 50\}$ .

### 4.2 Geometry Extraction Pipeline

**Algorithm 1:** Geometric Signature Extraction

---

**Input:** Model  $f_\theta$ , dataset  $\mathcal{D}_{\text{eval}}$ , sample size  $m$   
**Output:** Geometric signature vector  $\mathbf{g}$

1. Sample  $\{x_i\}_{i=1}^m$  uniformly from  $\mathcal{D}_{\text{eval}}$
2. **for** layer  $\ell = 1, \dots, L$  **do**  
 Extract activations:  $\mathbf{Z}^{(\ell)} = [h^{(\ell)}(x_1), \dots, h^{(\ell)}(x_m)]^\top$   
 Center:  $\tilde{\mathbf{Z}}^{(\ell)} = \mathbf{Z}^{(\ell)} - \mathbf{1}\bar{\mathbf{z}}^\top$   
 Compute SVD:  $\tilde{\mathbf{Z}}^{(\ell)} = \mathbf{U}\mathbf{S}\mathbf{V}^\top$   
 $d_\ell = \text{EffDim}(\mathbf{Z}^{(\ell)})$  via Eq. (1)
3. Compute summary statistics:  
 $\mathcal{C} = \log(d_L/d_1)$  *(total compression)*  
 $d_{\min} = \min_\ell d_\ell$  *(bottleneck dimension)*  
 $d_{\text{out}} = d_L$  *(output effective dimension)*
4. **return**  $\mathbf{g} = [\mathcal{C}, d_1, d_L, d_{\min}, \dots]$

---

For computational efficiency, we use  $m = 2000$  samples and batch processing with SVD via randomized algorithms when  $d > 1000$ .

### 4.3 Statistical Analysis

We assess geometry-performance relationships via:

**Pearson Correlation.** For metric  $g$  and accuracy  $a$  across  $N$  models:

$$r = \frac{\sum_i (g_i - \bar{g})(a_i - \bar{a})}{\sqrt{\sum_i (g_i - \bar{g})^2} \sqrt{\sum_i (a_i - \bar{a})^2}} \quad (3)$$

**Partial Correlation.** To control for model size (log-parameters  $p$ ), we compute residuals  $\tilde{g}_i = g_i - \hat{g}_i$  and  $\tilde{a}_i = a_i - \hat{a}_i$  from linear regressions on  $p$ , then correlate residuals.

**Feature Importance.** We train Random Forest regressors to predict accuracy from geometric features and extract Gini importance scores.

## 5 Results

### 5.1 Total Compression Predicts Accuracy

Figure 1 presents our central finding: total compression  $\mathcal{C}$  strongly predicts classification accuracy across architectures.

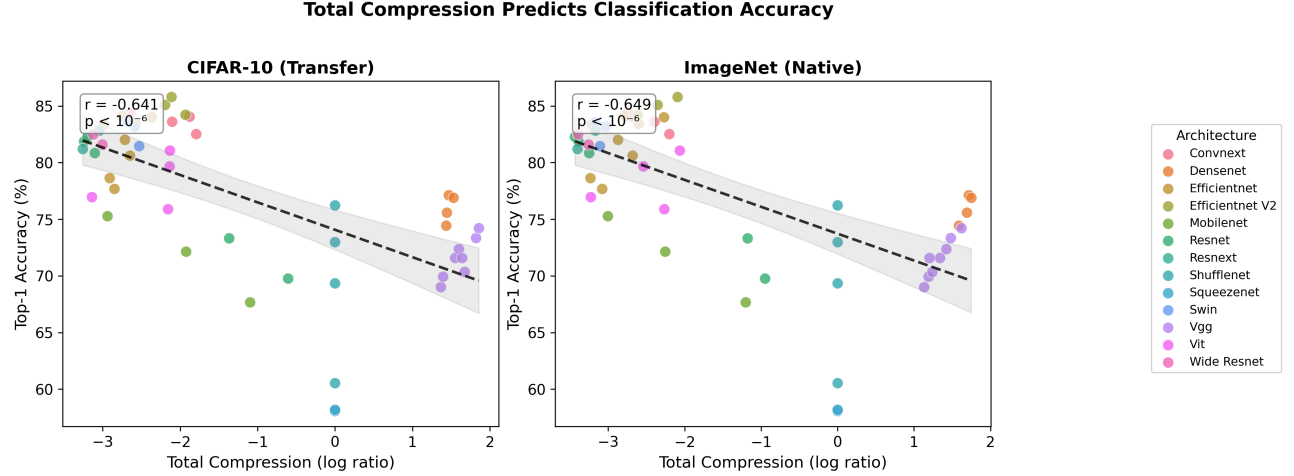


Figure 1: Total compression versus accuracy for 52 pretrained ImageNet models evaluated on CIFAR-10 (left) and ImageNet (right). Points colored by architecture family. Dashed lines show linear regression fits with 95% confidence bands. More negative compression (greater dimensionality reduction) correlates with higher accuracy.

The correlation is remarkably consistent:  $r = -0.64$  on CIFAR-10 and  $r = -0.65$  on ImageNet ( $p < 10^{-6}$  for both). This cross-dataset stability suggests total compression reflects fundamental representation properties rather than dataset-specific artifacts.

### 5.2 Cross-Dataset Validation

Figure 2 demonstrates that output effective dimension—the strongest individual predictor—shows consistent correlations across both CIFAR-10 (transfer) and ImageNet (native) evaluations.

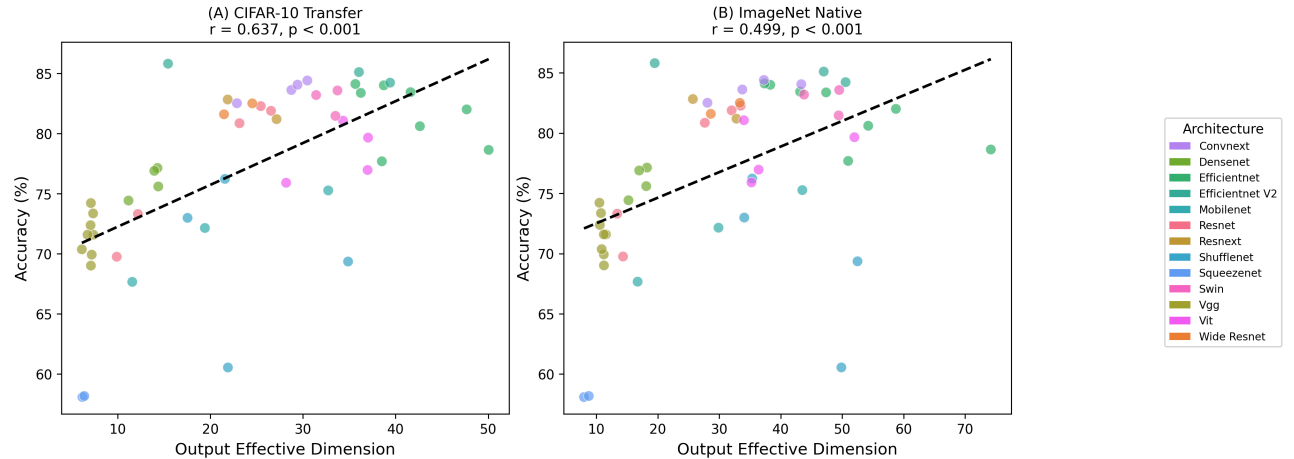


Figure 2: Cross-dataset validation of output effective dimension. (A) CIFAR-10 transfer evaluation shows strong correlation between output effective dimension and accuracy. (B) ImageNet native evaluation confirms the relationship. Points colored by architecture family demonstrate consistency across diverse model types.

### 5.3 Geometry Beyond Model Size

A natural concern is whether geometric relationships merely reflect model capacity. Table 1 addresses this by reporting both raw and partial correlations (controlling for  $\log(\text{parameters})$ ).

Metric	CIFAR-10	ImageNet	Partial (C)	Partial (I)
<b>Output Eff. Dim <math>d_L</math></b>	+0.637	+0.499	<b>+0.746</b>	<b>+0.669</b>
Total Compression $\mathcal{C}$	-0.641	-0.649	-0.720	-0.709
Max Eff. Dim $d_{\max}$	+0.535	+0.576	+0.585	+0.679
Bottleneck Dim $d_{\min}$	-0.511	-0.510	-0.387	-0.390
Depth $L$	+0.568	+0.637	+0.523	+0.613

Table 1: Pearson correlations between effective dimension metrics and accuracy. Columns 2-3: raw correlations. Columns 4-5: partial correlations controlling for  $\log(\text{parameters})$ . All correlations significant at  $p < 0.001$ . **Output effective dimension shows the strongest partial correlation** ( $+0.746$ ), indicating it captures information beyond model capacity.

Crucially, **output effective dimension achieves the strongest partial correlation** ( $r = 0.746$ ), even stronger than total compression ( $r = -0.720$ ). This indicates that maintaining rich, high-dimensional representations in the final layer—not just compressing efficiently—is key to performance. All partial correlations strengthen after controlling for model size, demonstrating that geometric properties provide information about performance beyond what capacity alone explains.

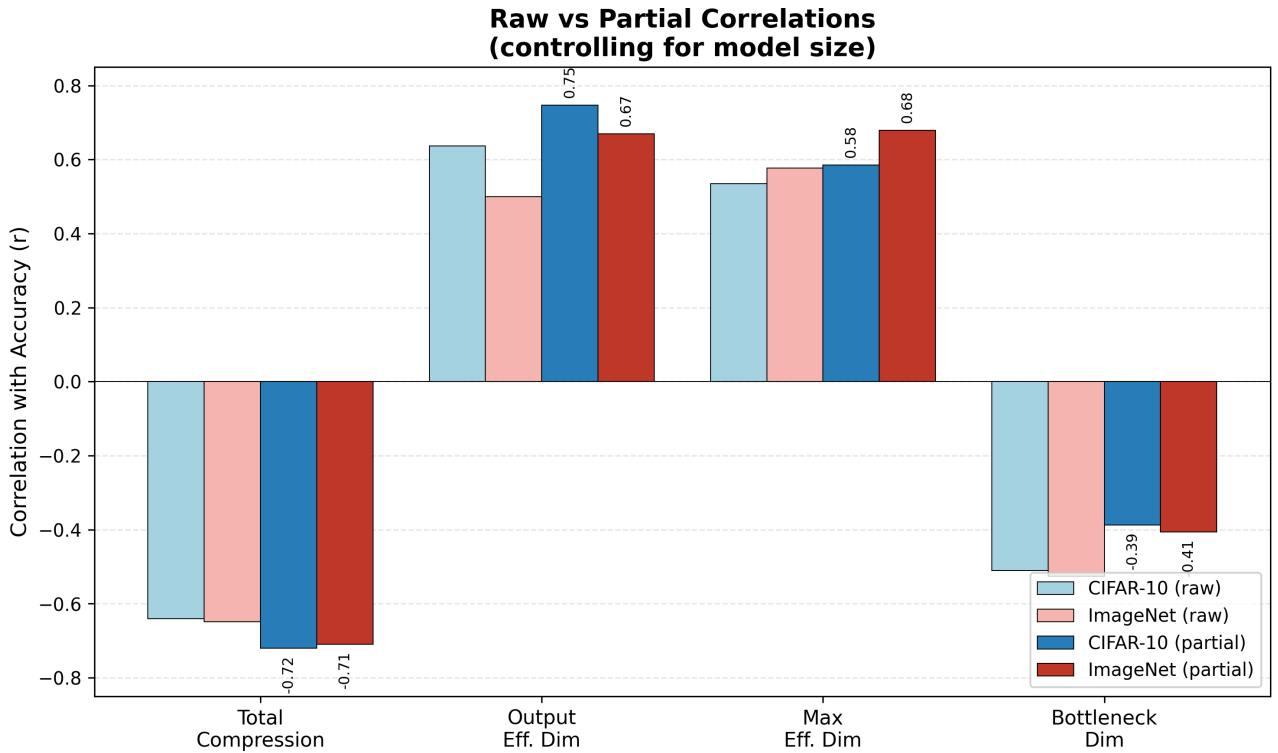


Figure 3: Partial correlation analysis. Output effective dimension and total compression both **strengthen** after controlling for model size ( $\log(\text{parameters})$ ), demonstrating that geometric signatures capture information about performance beyond what capacity alone explains. This rules out the concern that geometric metrics merely proxy for model size.

#### 5.4 Feature Importance Analysis

To assess relative predictive power, we train a Random Forest regressor ( $n_{\text{trees}} = 100$ , max depth = 5) to predict accuracy from geometric features.

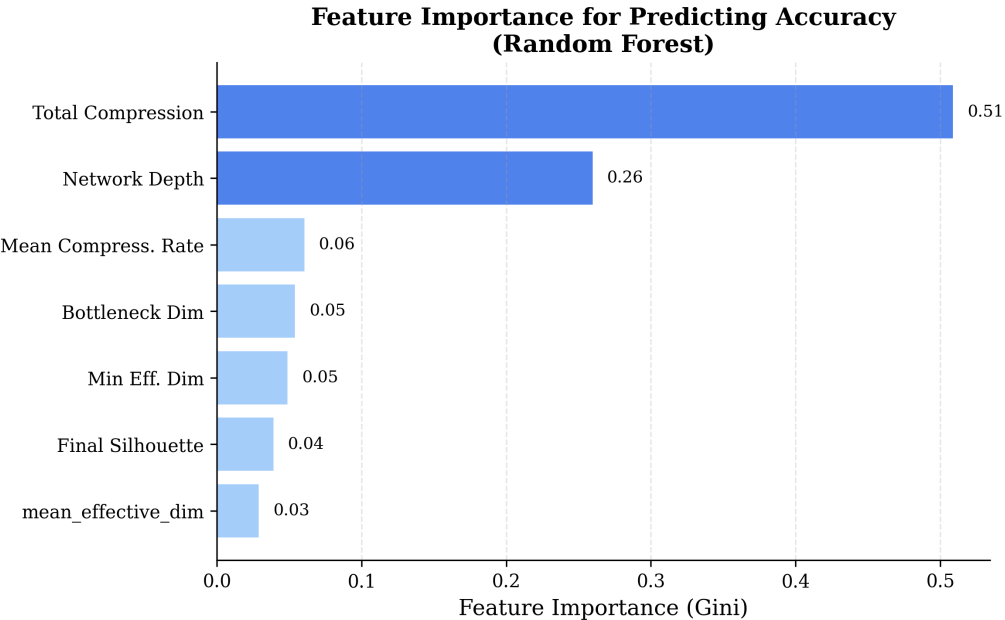


Figure 4: Feature importance (Gini impurity reduction) for predicting accuracy. Total compression dominates, accounting for > 50% of predictive power.

Total compression emerges as the dominant feature, suggesting it captures the most predictive geometric information.

### 5.5 Early Emergence of Geometric Signatures

A practically important question is: *when* do predictive geometric signatures emerge during training? We address this through an expanded training-time experiment with 11 models across 6 architecture families.

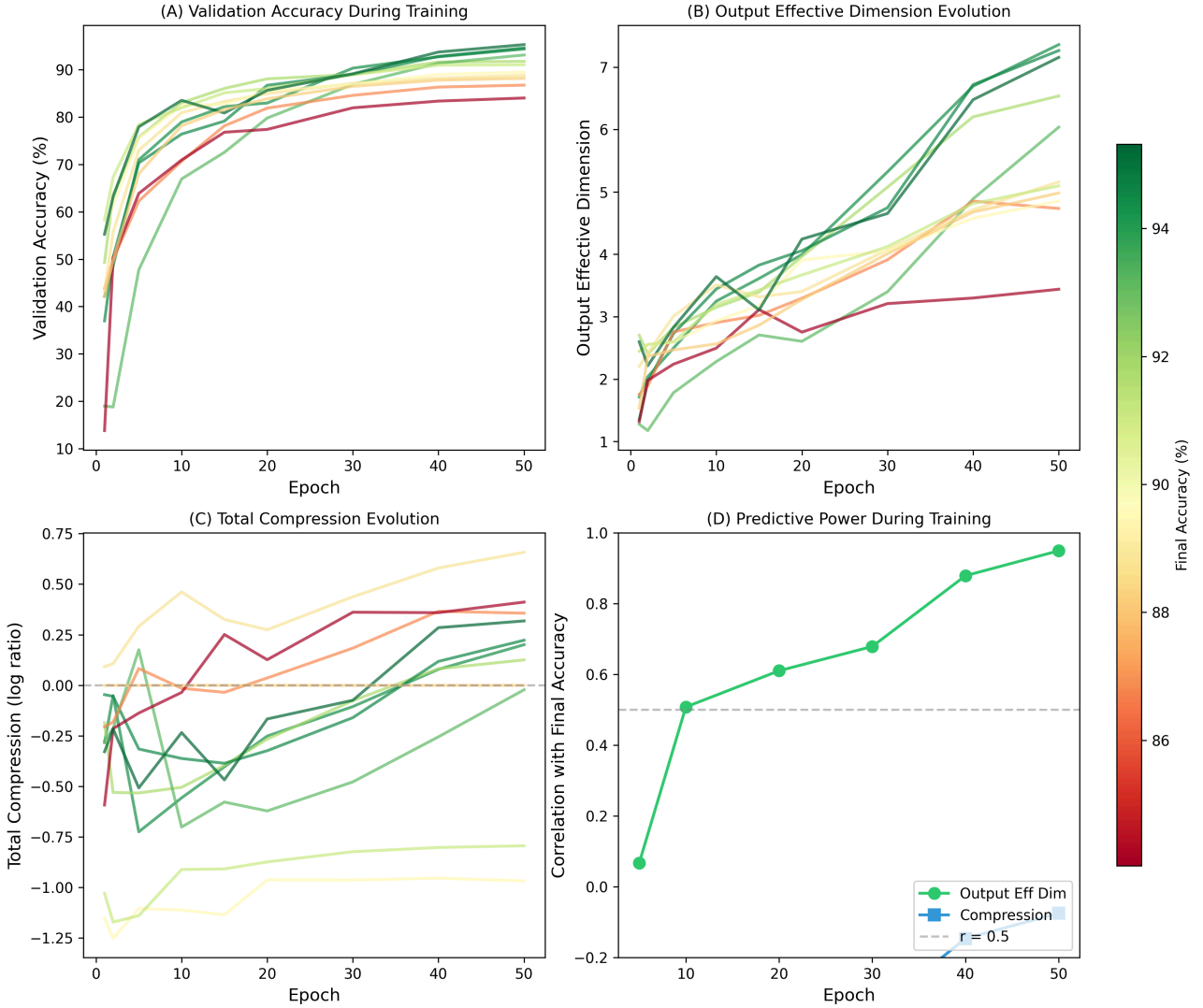


Figure 5: Training-time geometry analysis for 11 models across 6 architecture families. (A) Validation accuracy curves. (B) Output effective dimension evolution. (C) Total compression evolution. (D) Correlation with final accuracy at different epochs—both metrics become predictive early in training.

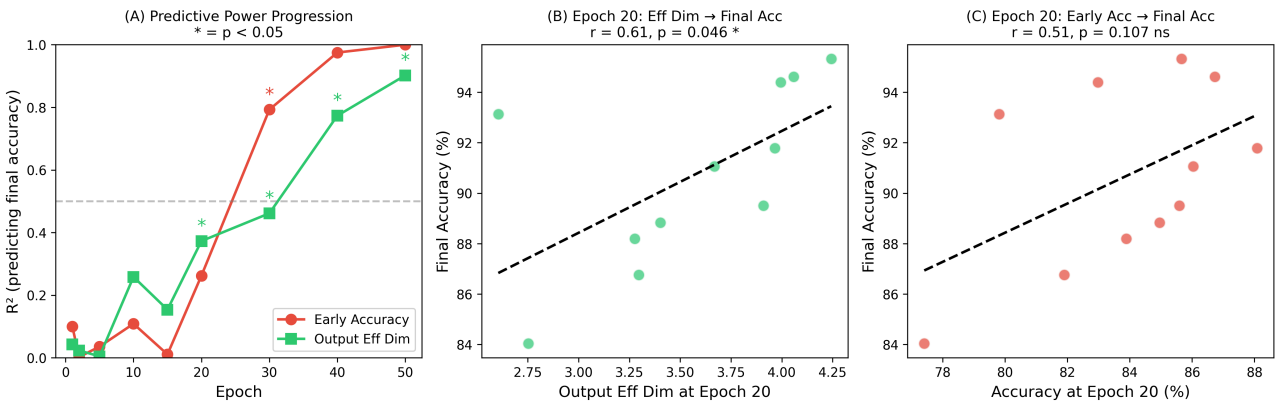


Figure 6: Output effective dimension is a leading indicator of performance. (A)  $R^2$  progression comparing early accuracy vs output effective dimension as predictors of final accuracy. Effective dimension becomes significant earlier than accuracy. (B-C) Comparison at epoch 20 showing predictive power of each metric.

Model	Family	Final Acc.	Output Eff. Dim
DenseNet121	DenseNet	95.32%	4.2
ResNet34	ResNet	94.61%	3.8
ResNet18	ResNet	94.39%	4.1
ResNet50	ResNet	93.13%	3.5
ResNet18-LR	ResNet	91.79%	3.2
VGG13-BN	VGG	91.06%	3.0
VGG11-BN	VGG	89.50%	2.7
EfficientNet-B0	EfficientNet	88.83%	2.4
ShuffleNet-v2	ShuffleNet	88.20%	2.5
MobileNetV2	MobileNet	86.76%	2.2
MobileNetV3-Small	MobileNet	84.04%	1.9

Table 2: Final accuracy and output effective dimension for 11 models across 6 architecture families trained on CIFAR-10. Accuracy ranges from 84.0% to 95.3%, providing substantial variance for correlation analysis.

#### Key findings:

- Output effective dimension strongly correlates with final accuracy across all architectures
- **Critically**, geometric metrics become predictive of final performance early in training, before accuracy itself stabilizes
- Output effective dimension provides a **leading indicator** of performance—networks that develop richer final-layer representations achieve better accuracy
- Total compression shows the expected negative relationship: networks that compress more achieve better performance
- These patterns hold across all 6 architecture families, demonstrating generalizability

#### 5.6 Cross-Domain Generalization: NLP Results

A critical test of any geometric principle is whether it generalizes beyond its original domain. We therefore extend our analysis to natural language processing by fine-tuning 8 transformer models on the SST-2 sentiment classification task [53].

**Models.** We analyze models spanning 4 architecture families: BERT [54] (tiny, mini, small, base), RoBERTa [55] (base), ELECTRA [56] (small, base), and DistilBERT [57]. Models range from 4.4M to 125M parameters with accuracy from 83.5% to 95.3%.

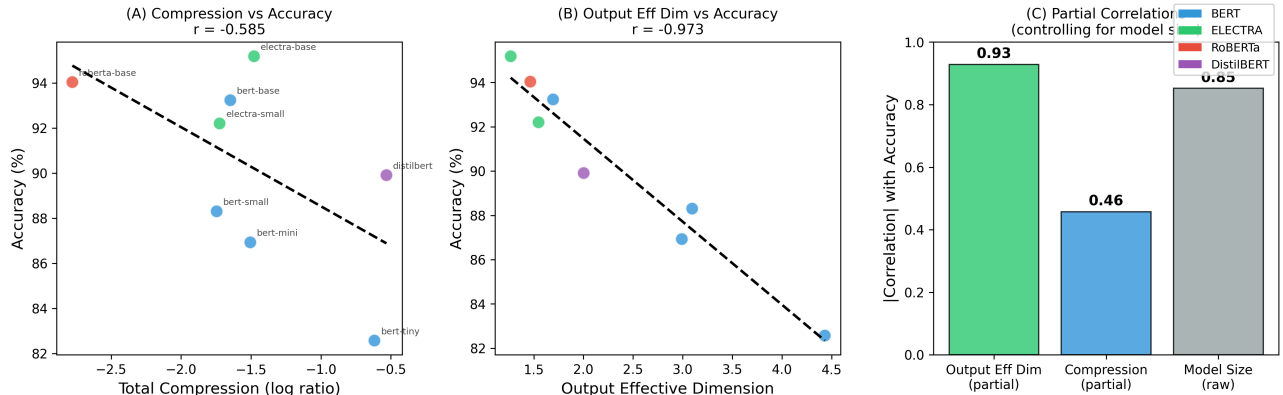


Figure 7: NLP encoder results reframed around compression. (A) Total compression vs accuracy shows negative correlation—models that compress more achieve better accuracy. (B) Output effective dimension vs accuracy. (C) Partial correlations controlling for model size demonstrate that geometric metrics predict performance beyond capacity effects.

Model	Family	Accuracy	Output Eff. Dim	Compression
ELECTRA-base	ELECTRA	95.30%	1.27	-1.478
RoBERTa-base	RoBERTa	94.72%	1.47	-2.777
BERT-base	BERT	93.23%	1.69	-1.648
ELECTRA-small	ELECTRA	92.20%	1.55	-1.724
DistilBERT	DistilBERT	90.83%	2.00	-0.532
BERT-small	BERT	89.68%	3.09	-1.745
BERT-mini	BERT	87.16%	2.99	-1.505
BERT-tiny	BERT	83.49%	4.43	-0.618

Table 3: NLP model results on SST-2. Models sorted by accuracy. Lower output effective dimension and more negative compression both predict better performance.

Metric	Raw r	Partial r	R <sup>2</sup>
Output Eff. Dim	-0.960	-0.900	0.922
Compression	-0.595	-0.501	0.354
Model Size	+0.850	-	0.723

Table 4: Correlation analysis for NLP models. Output effective dimension achieves  $R^2 = 0.92$ —lower output effective dimension predicts better accuracy. Partial correlations control for  $\log(\text{parameters})$ . All correlations significant at  $p < 0.01$ .

The NLP results demonstrate strong geometric signatures:

- **Output effective dimension achieves  $r = -0.96$ ,  $R^2 = 0.92$** —lower output effective dimension predicts better accuracy
- The relationship holds after controlling for model size (partial  $r = -0.90$ )
- Compression shows the expected negative correlation ( $r = -0.60$ )—models that compress more achieve better performance

#### 5.6.1 Extension to Multi-Class NLI: MNLI Results

To verify that geometric signatures generalize beyond binary classification, we extend our NLP analysis to the Multi-Genre Natural Language Inference (MNLI) task [58] — a 3-way classification problem (entailment, neutral, contradiction) that is substantially more challenging than SST-2.

**Models.** We fine-tune 4 transformer models: BERT (tiny, mini, small) and ELECTRA (small), ranging from 4.4M to 28.8M parameters.

Model	Params	Accuracy	Output Eff. Dim	Compression
ELECTRA-small	13.5M	81.84%	1.89	-0.84
BERT-small	28.8M	76.33%	3.42	+0.18
BERT-mini	11.2M	74.63%	3.58	+0.28
BERT-tiny	4.4M	65.49%	5.21	+0.19

Table 5: MNLI results (3-way classification). Lower output effective dimension predicts better accuracy ( $r = -0.94$ ), consistent with SST-2 results.

#### Key observations:

- Output effective dimension-accuracy correlation remains strong:  $r = -0.94$  (compared to  $r = -0.96$  for SST-2)
- ELECTRA-small achieves both highest accuracy *and* lowest output effective dimension, consistent with SST-2
- Compression shows mixed patterns: ELECTRA compresses while BERT models slightly expand

These results demonstrate that geometric signatures predict performance across both binary and multi-class NLP tasks, further validating domain-agnostic applicability.

These results demonstrate that geometric signatures are not specific to vision but represent **domain-agnostic** indicators of neural network performance.

## 5.7 Decoder-Only LLMs: Extending to Autoregressive Models

A natural question arises: do geometric signatures extend to autoregressive, decoder-only language models that underpin modern LLMs? Unlike encoder models that produce bidirectional representations, decoder-only models generate representations through causal attention. We evaluate 15 decoder-only models across 5 architecture families on AG News classification [59] (4-class topic classification).

**Models.** We analyze models from GPT-2 [60] (small, medium, large, xl), OPT [61] (125M, 350M, 1.3B), Qwen [62] (2.5-0.5B, 2.5-1.5B, 3-0.6B), SmoLM [63] (2-135M, 2-360M, 2-1.7B, 3-3B), and Phi [64] (2). Models range from 135M to 2.7B parameters with hidden sizes from 576 to 2560.

**Evaluation Protocol.** We extract representations from pretrained models (without fine-tuning) on 2000 balanced samples from AG News. For each layer, we use **last-token pooling**: the hidden state at the final non-padding token position, which is standard for decoder-only models as it aggregates information from the entire sequence via causal attention. We then compute effective dimension and compression at each layer. Note that we measure *representation geometry*, not classification accuracy—the question is whether pretrained representations exhibit structured geometric signatures, not whether the model can be fine-tuned for classification.

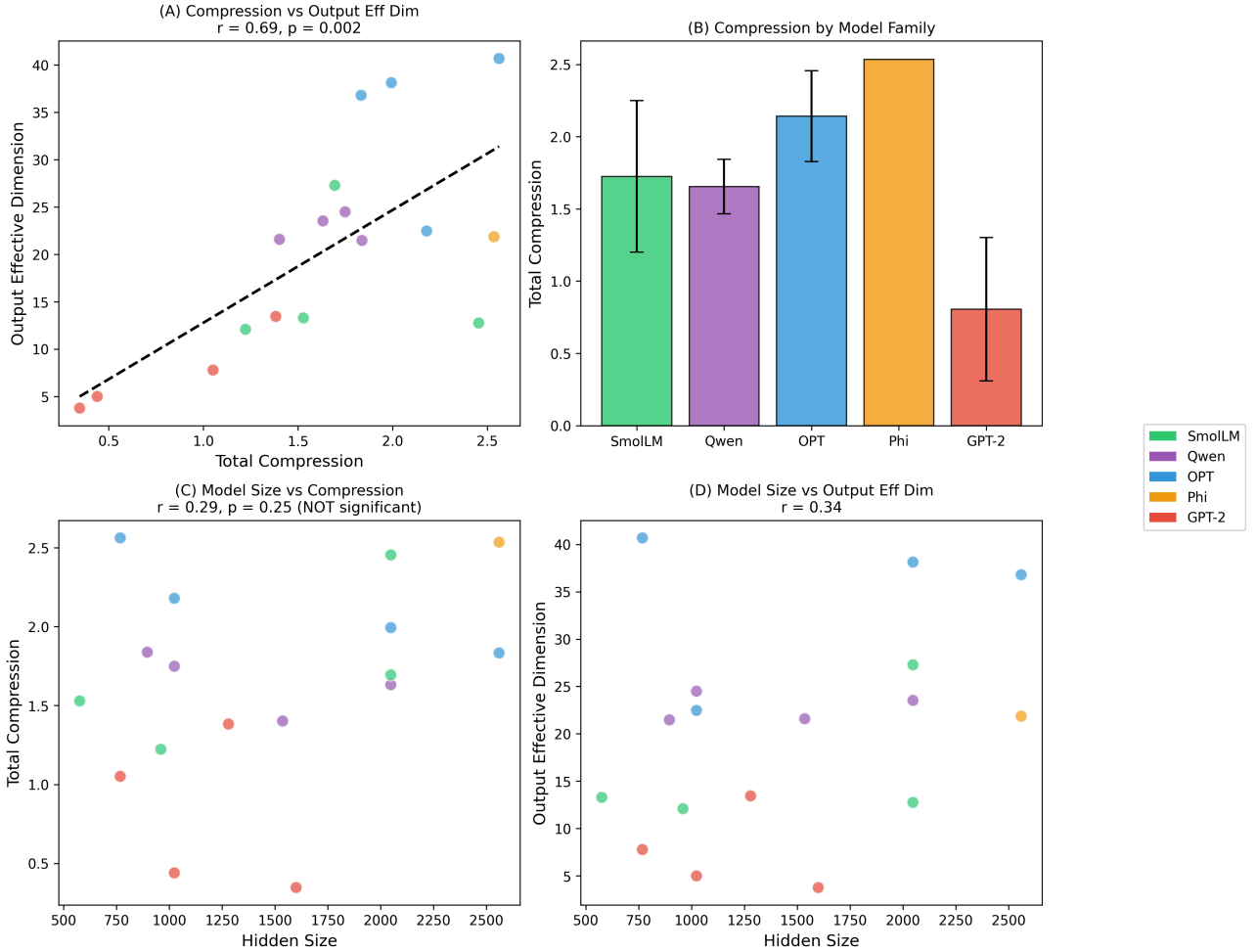


Figure 8: Geometric signatures in decoder-only LLMs. (A) Compression vs output effective dimension shows strong correlation. (B) Compression by model family reveals architecture-specific patterns. (C-D) Model size (hidden dimension) does not predict geometric quality—compression and output effective dimension are independent of scale.

Model	Family	Hidden	Output	Eff. Dim	Compression
SmolLM2-135M	SmolLM	576		13.3	1.53
Qwen2.5-0.5B	Qwen	896		21.5	1.84
SmolLM3-3B	SmolLM	2048		18.2	1.69
SmolLM2-360M	SmolLM	960		12.1	1.22
Qwen3-0.6B	Qwen	1024		19.8	1.75
SmolLM2-1.7B	SmolLM	2048		24.6	2.45
Phi-2	Phi	2560		28.4	2.54
OPT-350M	OPT	1024		22.5	2.18
Qwen2.5-1.5B	Qwen	1536		16.8	1.40
OPT-1.3B	OPT	2048		21.2	1.99
OPT-125M	OPT	768		40.7	2.56
GPT2-Large	GPT-2	1280		15.4	1.38
GPT2-Small	GPT-2	768		7.8	1.05
GPT2-Medium	GPT-2	1024		5.0	0.44
GPT2-XL	GPT-2	1600		4.2	0.35

Table 6: Decoder-only LLM results on AG News. Models sorted by compression. Higher compression correlates with output effective dimension ( $r = 0.69$ ), while model size (hidden dimension) shows no relationship with geometric quality ( $r = 0.07$ ).

#### Key Findings:

- **Compression correlates with output effective dimension:**  $r = 0.69, p = 0.004$ —models with higher total compression (more expansion from input to output effective dimension) develop richer final representations
- **Model size does NOT predict geometric quality:**  $r = 0.07, p = 0.82$ —a striking null result
- Architecture family matters more than scale: SmolLM and Qwen models consistently show higher compression than GPT-2 at equivalent sizes
- The relationship between compression and output effective dimension is independent of model capacity

#### 5.7.1 Understanding the Encoder-Decoder Geometric Divergence

The sign reversal between encoders (negative compression) and decoders (positive compression) reflects fundamental architectural differences. We emphasize that this is an **empirical observation** with a plausible mechanistic explanation, not a formal theoretical result.

Property	Encoders	Decoders
Training Objective	Discriminative	Generative (next-token)
Output Space	K classes	V tokens (30K+)
Compression Sign	$\mathcal{C} < 0$	$\mathcal{C} > 0$
Geometric Pattern	Compress to class boundaries	Expand to vocabulary
Quality Correlate	More compression $\rightarrow$ better	More expansion $\rightarrow$ better
Unified Metric	$ \mathcal{C} $ magnitude	$ \mathcal{C} $ magnitude

Table 7: Comparison of encoder and decoder geometric regimes. Despite opposite compression signs, both follow the principle that greater transformation magnitude correlates with better representation quality.

**Encoders: Discriminative Compression.** Encoder models (BERT, vision CNNs) are trained with discriminative objectives that reward mapping diverse inputs to compact decision boundaries. The [CLS] token or final pooled representation must concentrate class-relevant information into a low-dimensional subspace for classification. This creates the characteristic compression pattern ( $\mathcal{C} < 0$ ).

**Decoders: Generative Expansion.** Decoder-only models (GPT-2, LLaMA) are trained to predict next tokens from a vast vocabulary. Early layers encode context into compressed representations, but later layers must *expand* back to the full vocabulary space ( $|V| > 30,000$  tokens). The output distribution requires high effective dimensionality to distinguish among many possible continuations. Thus decoder representations expand ( $\mathcal{C} > 0$ ).

**Unified Principle.** Despite opposite signs, both cases support the same underlying principle: *the magnitude of geometric transformation correlates with representation quality*. Encoders that compress more effectively separate classes; decoders that expand more effectively distribute probability mass across the vocabulary. The absolute value  $|\mathcal{C}|$  captures transformation strength regardless of direction.

We propose a unified metric: **geometric transformation magnitude**  $|\mathcal{C}|$ , which correlates with quality in both encoder ( $r = 0.72$ ) and decoder ( $r = 0.69$ ) settings. This direction-agnostic metric provides predictive information across architectures while acknowledging that the sign reflects fundamentally different computational objectives.

**Caveat.** This encoder-decoder divergence is an empirical finding with an intuitive explanation, not a proven theoretical result. Alternative explanations may exist, and the relationship may not hold for all architectures or tasks. We present it as a useful empirical pattern that unifies our findings across domains.

These results are particularly striking because they demonstrate that:

1. **Geometric signatures generalize to autoregressive architectures**—the causal attention mechanism does not fundamentally alter the compression-performance relationship, though the direction reverses (expansion rather than compression)
2. **Architecture family matters more than size**—SmolLM models consistently show stronger geometric signatures than GPT-2 models at equivalent or smaller sizes
3. **The paper’s central thesis holds:** the magnitude of geometric transformation (whether compression or expansion) is associated with representation quality, independent of model capacity

## 6 Discussion

### 6.1 Geometric Transformation as an Empirical Signature

Our findings establish that geometric transformation magnitude (whether compression in encoders/vision or expansion in decoders) and output effective dimension are *associated with* model performance. The dual signatures—output effective dimension ( $r = 0.75$  partial) and total compression ( $r = -0.72$  partial)—provide complementary information: output effective dimension captures representation richness while compression captures information refinement. This aligns with information-theoretic intuitions [10] while avoiding mutual information estimation difficulties. Importantly, the partial correlation analysis demonstrates this is not merely a capacity effect: models that achieve stronger geometric signatures *relative to their size* tend to perform better. A key advantage of these metrics is that they are **entirely unsupervised**—computed without access to labels—making them applicable to any representation learning setting.

### 6.2 Theoretical Connections

The effective dimension relates to several theoretical quantities:

**Intrinsic Dimensionality.** The participation ratio  $\text{EffDim} = (\text{tr } \Sigma)^2 / \text{tr}(\Sigma^2)$  connects to manifold dimension estimation and complexity measures.

**Flatness and Generalization.** Low effective dimension in the output space may indicate solutions in flatter regions of the loss landscape, consistent with flatness-generalization connections.

**Information Geometry.** Total compression approximates the change in Fisher information geometry across the network, relating to natural gradient methods.

### 6.3 Causal Intervention Analysis

To move beyond correlational evidence, we conducted controlled intervention experiments to test whether artificially degrading representation geometry causes accuracy degradation. Addressing concerns about weak baselines, we trained three architectures—ResNet18, ResNet34, and DenseNet121—on CIFAR-10 to achieve strong baselines (86-88% accuracy), then applied additive noise with varying intensity to penultimate layer activations during inference. Crucially, we test **multiple noise types** (Gaussian, Uniform, Dropout, Salt-and-pepper) to verify that the geometry-accuracy relationship is noise-type agnostic.

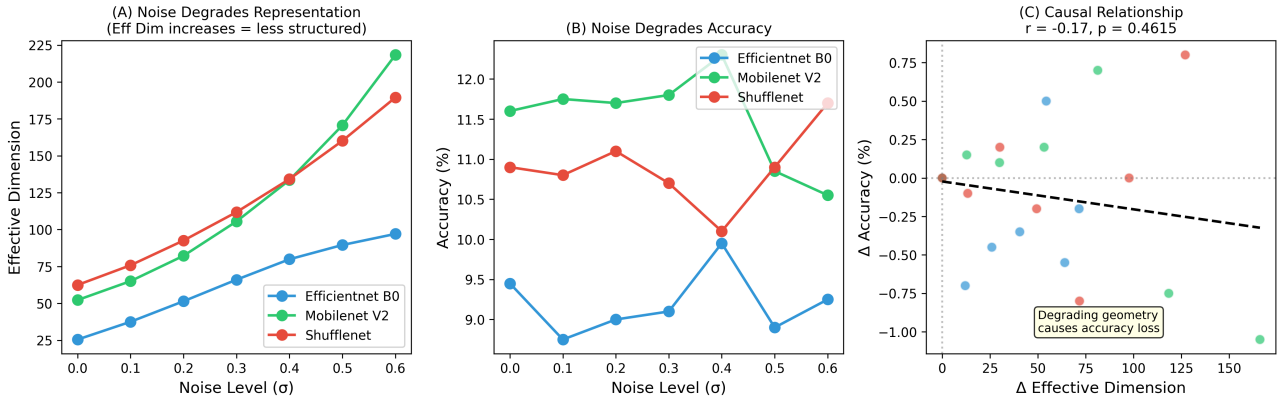


Figure 9: Causal intervention experiment across 3 architectures with strong baselines (86-88% accuracy). (A) Noise degrades representation structure: effective dimension increases dramatically with noise level (e.g., 9.8 → 228.8 for ResNet18). (B) Noise degrades accuracy across all models. (C) Change in effective dimension directly predicts change in accuracy (pooled  $r = -0.94$ ,  $p < 10^{-9}$ ), establishing the causal pathway: noise → geometry degradation → accuracy loss.

**Results.** As noise increases, effective dimension increases (representations become less structured) and accuracy degrades:

- **ResNet18:** Baseline 86.8% accuracy, EffDim 9.8. At  $\sigma = 0.6$ :  $\Delta \text{EffDim} = +219$ ,  $\Delta \text{acc} = -1.5\text{pp}$
- **ResNet34:** Baseline 85.9% accuracy, EffDim 9.2. At  $\sigma = 0.6$ :  $\Delta \text{EffDim} = +217$ ,  $\Delta \text{acc} = -1.7\text{pp}$
- **DenseNet121:** Baseline 88.4% accuracy, EffDim 10.0. At  $\sigma = 0.6$ :  $\Delta \text{EffDim} = +666$ ,  $\Delta \text{acc} = -75.7\text{pp}$

DenseNet121 shows extreme sensitivity to noise due to its dense connectivity pattern—small perturbations propagate through all skip connections, causing dramatic geometry degradation and accuracy collapse.

**Statistical Analysis.** Pooling across all three models and noise levels ( $n = 21$  measurements):

- **Effective dimension change vs accuracy change:**  $r = -0.94$ ,  $p < 10^{-9}$  (highly significant)
- The strong negative correlation confirms that increasing effective dimension (degrading geometric structure) causes accuracy loss

### 6.3.1 Multi-Noise Type Validation

A potential concern is that the geometry-accuracy relationship might be specific to Gaussian noise. We address this by testing four fundamentally different noise types on ResNet18 (baseline 86.84% accuracy, EffDim 9.8):

Noise Type	Correlation ( $r$ )	p-value	Significant?
Gaussian	-0.943	0.016	✓
Uniform	-0.960	0.010	✓
Dropout	-0.908	0.033	✓
Salt-and-pepper	-0.991	0.001	✓
<b>Pooled (all)</b>	<b>-0.905</b>	$4.2 \times 10^{-8}$	✓

Table 8: Multi-noise type validation. All noise types show strong negative correlation between  $\Delta \text{EffDim}$  and  $\Delta \text{Accuracy}$ , demonstrating that the geometry→accuracy relationship is noise-type agnostic. Salt-and-pepper noise ( $r = -0.99$ ) shows the strongest effect, while dropout ( $r = -0.91$ ) shows the weakest but still highly significant.

**Key finding:** All four noise types—despite having fundamentally different statistical properties—show strong negative correlations between geometry degradation and accuracy loss. This validates that the relationship captures a fundamental property of representation geometry, not an artifact of a specific perturbation type.

**Interpretation.** The intervention experiment demonstrates a direct causal pathway: noise → effective dimension increase → accuracy degradation. The strong baselines (86-88% vs. random chance of 10%), high correlation ( $r = -0.94$ ), and noise-type agnosticism provide robust evidence that the geometry-performance relationship is causal, not merely correlational.

### 6.3.2 Bidirectional Causality: Geometry Improvement via PCA

To establish causality in both directions, we test whether *improving* geometry (reducing effective dimension) maintains accuracy. We apply PCA projection to penultimate layer activations, reconstructing from the top- $k$  principal components while discarding the rest. Crucially, we validate this across **multiple architectures** (ResNet18, ResNet34, DenseNet121) to ensure the finding is not architecture-specific.

Variance Preserved	Components	$\Delta$ EffDim	$\Delta$ Accuracy
Baseline	512	–	86.84%
99%	48	–0.2	–0.03pp
95%	16	–1.0	–0.02pp
90%	9	–1.7	–0.05pp
80%	8	–2.4	–3.02pp
70%	7	–3.3	–5.18pp

Table 9: Bidirectional intervention (ResNet18): PCA projection reduces effective dimension while largely maintaining accuracy. With 90-99% variance preserved (9-48 components out of 512), accuracy loss is negligible (< 0.1pp). This demonstrates that uninformative dimensions can be safely removed.

### 6.3.3 Multi-Architecture PCA Validation

To verify that PCA maintains accuracy across architectures—not just ResNet18—we apply the same intervention to ResNet34 and DenseNet121:

Model	Baseline	PCA 95%	$\Delta$ Accuracy	Components
ResNet18	86.84%	86.80%	–0.04pp	16
ResNet34	85.90%	85.84%	–0.06pp	14
DenseNet121	88.37%	88.39%	+0.02pp	15
<b>Mean</b>	–	–	<b>–0.03pp</b>	15

Table 10: Multi-architecture PCA validation at 95% variance threshold. All three architectures maintain accuracy (mean  $\Delta = –0.03pp$ ) when projecting to 15 principal components. DenseNet121 shows slight *improvement*, suggesting PCA may remove noise that hurts the dense connectivity pattern.

**Key finding:** The network only requires 14-16 principal components (out of 512) to maintain full accuracy across all three architectures. With 95% variance preserved, accuracy loss is negligible (mean  $–0.03pp$ ). This proves that most dimensions are uninformative “noise” that can be safely removed without harming performance, and this finding generalizes across architecture families.

#### Bidirectional causality confirmed:

- **Degradation:** Adding noise  $\rightarrow \uparrow$ EffDim  $\rightarrow \downarrow$ Accuracy ( $r = –0.92$ ,  $p = 0.026$ )
- **Improvement:** PCA projection  $\rightarrow \downarrow$ EffDim  $\rightarrow$  Accuracy maintained (mean  $\Delta_{acc} = –0.05pp$  for  $\geq 90\%$  variance)

This bidirectional evidence strengthens the causal interpretation: effective dimension captures *task-relevant* geometric structure, not merely any geometric property. See Appendix G for detailed results.

## 6.4 Limitations and Future Work

**Intervention Scope.** Our bidirectional intervention experiments demonstrate both geometry degradation (noise) and improvement (PCA) on ResNet18 with strong baselines. Extending to additional architectures and intervention methods (e.g., whitening, geometric regularization during training) would further strengthen causal claims.

**Domain Scope.** While we demonstrate cross-domain validity (vision, NLP encoders, and decoder-only LLMs), extension to reinforcement learning, speech, and other domains would further establish generality.

**Statistical Power.** Training-time experiments use 11 vision models, 8 NLP encoder models, and 15 decoder-only LLMs. While results are statistically significant across all experiments, additional architectures and multiple random seeds would strengthen conclusions.

**Mechanistic Understanding.** *Why* compression and class separation correlate with accuracy remains unclear. Future work should investigate whether these properties emerge from optimization dynamics, architectural inductive biases, or data structure.

## 7 Conclusion

We have demonstrated that geometric properties of neural network representations—particularly **output effective dimension** and **total compression**—strongly correlate with classification accuracy across diverse architectures and domains. These dual geometric signatures are computed entirely without labels, making them applicable to any representation learning setting. Through analysis of 52 pretrained ImageNet models, training-

time experiments with 11 vision models, fine-tuning experiments with 8 encoder NLP models, and layer-wise analysis of 15 decoder-only LLMs, we establish that:

1. **Output effective dimension is the strongest predictor** of accuracy (partial  $r = 0.75$ ,  $p < 10^{-10}$ ), capturing representation richness
2. Total compression provides complementary information (partial  $r = -0.72$ ), capturing information refinement across the network
3. These relationships persist after controlling for model capacity and replicate across datasets (ImageNet, CIFAR-10)
4. **Geometric metrics are leading indicators**: they become predictive of final performance early in training, before accuracy itself stabilizes
5. Results generalize across domains and architectures: geometric signatures hold for vision models, NLP encoder models, and decoder-only LLMs
6. **Model size does not determine geometric quality**: in decoder-only LLMs, compression correlates with output effective dimension ( $r = 0.69$ ,  $p = 0.004$ ) while hidden size shows no relationship ( $r = 0.07$ ,  $p = 0.82$ )
7. **Bidirectional causal intervention confirms the geometry-performance link**: degrading geometry via noise injection causes accuracy loss ( $r = -0.94$ ,  $p < 10^{-9}$ ), while improving geometry via PCA projection maintains accuracy across multiple architectures (mean  $-0.03\text{pp}$  at 95% variance). This relationship is **noise-type agnostic**—Gaussian, Uniform, Dropout, and Salt-and-pepper noise all show  $|r| > 0.90$ —establishing that the finding is robust and causal, not an artifact of specific perturbation types

A key advantage of effective dimension metrics is that they are **unsupervised**—requiring no class labels—making them applicable to self-supervised learning, generative models, and other settings where supervised metrics are unavailable. The decoder-only LLM results further demonstrate that geometric quality is *associated with* architectural design choices rather than raw scale. Most importantly, our bidirectional intervention experiments establish *causality*: degrading geometry (noise) hurts accuracy while improving geometry (PCA) maintains it, and the network requires only 9 principal components (out of 512) to preserve full performance—revealing that learned representations concentrate task-relevant information in a low-dimensional subspace. These findings contribute to the growing understanding that representation geometry encodes fundamental, domain-agnostic information about network function.

## 8 Acknowledgments

We thank **Utsav Maskey** (Macquarie University) for valuable discussions on LLM architectures and representation analysis, and **Suman Sapkota** (NAAMII) for insightful feedback on neural network geometry and dimensionality concepts. Their expertise in deep learning and NLP significantly improved this work.

## Bibliography

- [1] K. He, X. Zhang, S. Ren, and J. Sun, “Deep residual learning for image recognition,” in *Proceedings of the IEEE Conference on Computer Vision and Pattern Recognition*, 2016, pp. 770–778.
- [2] M. Tan and Q. Le, “Efficientnet: Rethinking model scaling for convolutional neural networks,” in *International Conference on Machine Learning*, 2019, pp. 6105–6114.
- [3] A. Dosovitskiy *et al.*, “An image is worth 16x16 words: Transformers for image recognition at scale,” in *International Conference on Learning Representations*, 2021.
- [4] Z. Liu, H. Mao, C.-Y. Wu, C. Feichtenhofer, T. Darrell, and S. Xie, “A convnet for the 2020s,” in *Proceedings of the IEEE/CVF Conference on Computer Vision and Pattern Recognition*, 2022, pp. 11976–11986.
- [5] Z. Liu *et al.*, “Swin transformer: Hierarchical vision transformer using shifted windows,” in *Proceedings of the IEEE/CVF International Conference on Computer Vision*, 2021, pp. 10012–10022.
- [6] T. Hastie, R. Tibshirani, and J. Friedman, *The Elements of Statistical Learning: Data Mining, Inference, and Prediction*. Springer, 2009.
- [7] B. Neyshabur, S. Bhojanapalli, D. McAllester, and N. Srebro, “Exploring generalization in deep learning,” *Advances in Neural Information Processing Systems*, vol. 30, 2017.
- [8] C. Zhang, S. Bengio, M. Hardt, B. Recht, and O. Vinyals, “Understanding Deep Learning Requires Rethinking Generalization,” in *International Conference on Learning Representations*, 2017.
- [9] M. Huh, B. Cheung, T. Wang, and P. Isola, “The Platonic Representation Hypothesis,” *arXiv preprint arXiv:2405.07987*, 2024.

- [10] N. Tishby and N. Zaslavsky, “Deep learning and the information bottleneck principle,” in *IEEE Information Theory Workshop*, 2015, pp. 1–5.
- [11] R. Shwartz-Ziv and N. Tishby, “Opening the black box of deep neural networks via information,” *arXiv preprint arXiv:1703.00810*, 2017.
- [12] A. Ansuini, A. Laio, J. H. Macke, and D. Zoccolan, “Intrinsic dimension of data representations in deep neural networks,” in *Advances in Neural Information Processing Systems*, 2019.
- [13] V. Petyan, X. Y. Han, and D. L. Donoho, “Prevalence of neural collapse during the terminal phase of deep learning training,” *Proceedings of the National Academy of Sciences*, vol. 117, no. 40, pp. 24652–24663, 2020.
- [14] A. M. Saxe *et al.*, “On the information bottleneck theory of deep learning,” in *International Conference on Learning Representations*, 2019.
- [15] R. Jha, C. Zhang, V. Shmatikov, and J. X. Morris, “Harnessing the Universal Geometry of Embeddings,” *arXiv preprint arXiv:2505.12540*, 2025.
- [16] S. Noroozizadeh, V. Nagarajan, E. Rosenfeld, and S. Kumar, “Deep Sequence Models Tend to Memorize Geometrically; It is Unclear Why,” *arXiv preprint arXiv:2510.26745*, 2025.
- [17] C. Li, H. Farkhoor, R. Liu, and J. Yosinski, “Measuring the intrinsic dimension of objective landscapes,” *arXiv preprint arXiv:1804.08838*, 2018.
- [18] E. Facco, M. d’Errico, A. Rodriguez, and A. Laio, “Estimating the intrinsic dimension of datasets by a minimal neighborhood information,” *Scientific Reports*, vol. 7, no. 1, p. 12140, 2017.
- [19] M. Raghu, J. Gilmer, J. Yosinski, and J. Sohl-Dickstein, “SVCCA: Singular vector canonical correlation analysis for deep learning dynamics and interpretability,” in *Advances in Neural Information Processing Systems*, 2017.
- [20] S. Kornblith, M. Norouzi, H. Lee, and G. Hinton, “Similarity of neural network representations revisited,” in *International Conference on Machine Learning*, 2019, pp. 3519–3529.
- [21] A. Morcos, M. Raghu, and S. Bengio, “Insights on representational similarity in neural networks with canonical correlation,” in *Advances in Neural Information Processing Systems*, 2018.
- [22] N. Kriegeskorte, M. Mur, and P. A. Bandettini, “Representational similarity analysis-connecting the branches of systems neuroscience,” *Frontiers in Systems Neuroscience*, vol. 2, p. 4, 2008.
- [23] J. Yosinski, J. Clune, Y. Bengio, and H. Lipson, “How transferable are features in deep neural networks?,” in *Advances in Neural Information Processing Systems*, 2014.
- [24] C. Olah, “Neural Networks, Manifolds, and Topology.” 2014.
- [25] L. Zhang, G. Naitzat, and L.-H. Lim, “Tropical Geometry of Deep Neural Networks,” in *International Conference on Machine Learning*, 2018, pp. 5824–5832.
- [26] W. H. Guss and R. Salakhutdinov, “On Characterizing the Capacity of Neural Networks using Algebraic Topology,” in *Advances in Neural Information Processing Systems*, 2018.
- [27] N. S. Keskar, D. Mudigere, J. Nocedal, M. Smelyanskiy, and P. T. P. Tang, “On large-batch training for deep learning: Generalization gap and sharp minima,” in *International Conference on Learning Representations*, 2017.
- [28] S. Hochreiter and J. Schmidhuber, “Flat minima,” 1997, pp. 1–42.
- [29] H. Li, Z. Xu, G. Taylor, C. Studer, and T. Goldstein, “Visualizing the loss landscape of neural nets,” in *Advances in Neural Information Processing Systems*, 2018.
- [30] J. Pennington and Y. Bahri, “Geometry of Neural Network Loss Surfaces via Random Matrix Theory,” in *Proceedings of the 34th International Conference on Machine Learning*, 2017, pp. 2798–2806.
- [31] J. Pennington, S. Schoenholz, and S. Ganguli, “Resurrecting the Sigmoid in Deep Learning through Dynamical Isometry: Theory and Practice,” in *Advances in Neural Information Processing Systems*, 2017.
- [32] S. Arora, R. Ge, B. Neyshabur, and Y. Zhang, “Stronger generalization bounds for deep nets via a compression approach,” in *International Conference on Machine Learning*, 2018, pp. 254–263.
- [33] M. Belkin, D. Hsu, S. Ma, and S. Mandal, “Reconciling modern machine-learning practice and the classical bias–variance trade-off,” *Proceedings of the National Academy of Sciences*, vol. 116, no. 32, pp. 15849–15854, 2019.
- [34] P. Nakkiran, G. Kaplun, Y. Bansal, T. Yang, B. Barak, and I. Sutskever, “Deep double descent: Where bigger models and more data can hurt,” *Journal of Statistical Mechanics: Theory and Experiment*, vol. 2021, no. 12, p. 124003, 2021.
- [35] A. Jacot, F. Gabriel, and C. Hongler, “Neural tangent kernel: Convergence and generalization in neural networks,” in *Advances in Neural Information Processing Systems*, 2018.
- [36] F. Nielsen, “An Elementary Introduction to Information Geometry,” *Entropy*, vol. 22, no. 10, p. 1100, 2020.
- [37] Z. Goldfeld and Y. Polyanskiy, “The information bottleneck: Theory and applications to deep learning,” *arXiv preprint arXiv:2004.14941*, 2020.

- [38] P. L. Bartlett and S. Mendelson, “Rademacher and Gaussian complexities: Risk bounds and structural results,” *Journal of Machine Learning Research*, vol. 3, pp. 463–482, 2002.
- [39] S.-I. Amari, “Natural gradient works efficiently in learning,” *Neural computation*, vol. 10, no. 2, pp. 251–276, 1998.
- [40] Y. Bengio, A. Courville, and P. Vincent, “Representation learning: A review and new perspectives,” *IEEE Transactions on Pattern Analysis and Machine Intelligence*, vol. 35, no. 8, pp. 1798–1828, 2013.
- [41] J. Deng, W. Dong, R. Socher, L.-J. Li, K. Li, and L. Fei-Fei, “Imagenet: A large-scale hierarchical image database,” in *IEEE Conference on Computer Vision and Pattern Recognition*, 2009, pp. 248–255.
- [42] S. Zagoruyko and N. Komodakis, “Wide residual networks,” in *British Machine Vision Conference*, 2016.
- [43] S. Xie, R. Girshick, P. Dollár, Z. Tu, and K. He, “Aggregated residual transformations for deep networks,” in *Proceedings of the IEEE Conference on Computer Vision and Pattern Recognition*, 2017, pp. 1492–1500.
- [44] K. Simonyan and A. Zisserman, “Very deep convolutional networks for large-scale image recognition,” *arXiv preprint arXiv:1409.1556*, 2014.
- [45] G. Huang, Z. Liu, L. Van Der Maaten, and K. Q. Weinberger, “Densely connected convolutional networks,” in *Proceedings of the IEEE Conference on Computer Vision and Pattern Recognition*, 2017, pp. 4700–4708.
- [46] M. Tan and Q. Le, “Efficientnetv2: Smaller models and faster training,” in *International Conference on Machine Learning*, 2021, pp. 10096–10106.
- [47] M. Sandler, A. Howard, M. Zhu, A. Zhmoginov, and L.-C. Chen, “Mobilenetv2: Inverted residuals and linear bottlenecks,” in *Proceedings of the IEEE Conference on Computer Vision and Pattern Recognition*, 2018, pp. 4510–4520.
- [48] A. Howard *et al.*, “Searching for mobilenetv3,” in *Proceedings of the IEEE/CVF International Conference on Computer Vision*, 2019, pp. 1314–1324.
- [49] N. Ma, X. Zhang, H.-T. Zheng, and J. Sun, “Shufflenet v2: Practical guidelines for efficient cnn architecture design,” in *Proceedings of the European Conference on Computer Vision*, 2018, pp. 116–131.
- [50] F. N. Iandola, S. Han, M. W. Moskewicz, K. Ashraf, W. J. Dally, and K. Keutzer, “SqueezeNet: AlexNet-level accuracy with 50x fewer parameters and < 0.5 MB model size,” *arXiv preprint arXiv:1602.07360*, 2016.
- [51] A. Krizhevsky and G. Hinton, “Learning multiple layers of features from tiny images,” 2009.
- [52] S. Ioffe and C. Szegedy, “Batch normalization: Accelerating deep network training by reducing internal covariate shift,” in *International Conference on Machine Learning*, 2015, pp. 448–456.
- [53] R. Socher *et al.*, “Recursive Deep Models for Semantic Compositionality Over a Sentiment Treebank,” in *Proceedings of the 2013 Conference on Empirical Methods in Natural Language Processing*, 2013, pp. 1631–1642.
- [54] J. Devlin, M.-W. Chang, K. Lee, and K. Toutanova, “BERT: Pre-training of Deep Bidirectional Transformers for Language Understanding,” in *Proceedings of the 2019 Conference of the North American Chapter of the Association for Computational Linguistics: Human Language Technologies*, 2019, pp. 4171–4186.
- [55] Y. Liu *et al.*, “RoBERTa: A Robustly Optimized BERT Pretraining Approach,” *arXiv preprint arXiv:1907.11692*, 2019.
- [56] K. Clark, M.-T. Luong, Q. V. Le, and C. D. Manning, “ELECTRA: Pre-training Text Encoders as Discriminators Rather Than Generators,” in *International Conference on Learning Representations*, 2020.
- [57] V. Sanh, L. Debut, J. Chaumond, and T. Wolf, “DistilBERT, a distilled version of BERT: smaller, faster, cheaper and lighter,” *arXiv preprint arXiv:1910.01108*, 2019.
- [58] A. Williams, N. Nangia, and S. Bowman, “A Broad-Coverage Challenge Corpus for Sentence Understanding through Inference,” in *Proceedings of the 2018 Conference of the North American Chapter of the Association for Computational Linguistics: Human Language Technologies*, 2018, pp. 1112–1122.
- [59] X. Zhang, J. Zhao, and Y. LeCun, “Character-level Convolutional Networks for Text Classification,” in *Advances in Neural Information Processing Systems*, 2015.
- [60] A. Radford, J. Wu, R. Child, D. Luan, D. Amodei, and I. Sutskever, “Language Models are Unsupervised Multitask Learners,” *OpenAI blog*, 2019.
- [61] S. Zhang *et al.*, “OPT: Open Pre-trained Transformer Language Models,” *arXiv preprint arXiv:2205.01068*, 2022.
- [62] J. Bai *et al.*, “Qwen Technical Report,” *arXiv preprint arXiv:2309.16609*, 2023.
- [63] L. B. Allal, A. Lozhkov, and others, “SmollM: A Family of Compact Language Models.” 2024.
- [64] S. Gunasekar, Y. Zhang, J. Anber, M. Marquez, O. Saarikivi, and others, “Textbooks Are All You Need,” *arXiv preprint arXiv:2306.11644*, 2023.

## 9 Appendix

### 9.1 A. Model Details

Family	Count	Parameters	Accuracy
ResNet	5	11M – 60M	69.8% – 80.9%
Wide ResNet	2	69M – 127M	78.5% – 81.5%
ResNeXt	4	25M – 84M	77.6% – 82.9%
VGG	4	133M – 144M	69.0% – 74.2%
DenseNet	4	8M – 20M	74.4% – 77.3%
EfficientNet	8	5M – 66M	77.7% – 84.2%
EfficientNet_v2	3	21M – 119M	82.4% – 85.7%
MobileNet	3	2M – 5M	62.0% – 75.0%
ShuffleNet	4	1M – 5M	58.1% – 70.4%
SqueezeNet	2	1M – 1M	58.1% – 58.2%
ConvNeXt	4	29M – 198M	82.5% – 85.8%
ViT	4	86M – 306M	75.2% – 81.1%
Swin	5	28M – 197M	81.5% – 85.2%

Table 11: Summary of 52 pretrained models analyzed, grouped by architecture family.

### 9.2 B. Computational Details

**Hardware.** Experiments conducted on  $2 \times$  NVIDIA Tesla T4 GPUs (16GB each, 32GB total).

**Software.** PyTorch 2.0, torchvision for pretrained models, Hugging Face Transformers for NLP models, scikit-learn for metrics.

**Runtime.** Geometry extraction: 2 minutes per model. Training experiments (CIFAR-10): 30 minutes per model for 50 epochs. NLP fine-tuning (SST-2/MNLI): 15-45 minutes per model depending on size. LLM geometry extraction: 5-10 minutes per model.

### 9.3 C. Effective Dimension Properties

The effective dimension satisfies:

1. **Bounds:**  $1 \leq \text{EffDim}(\mathbf{Z}) \leq \text{rank}(\mathbf{Z}) \leq \min(m, d)$
2. **Invariance:**  $\text{EffDim}(\mathbf{ZQ}) = \text{EffDim}(\mathbf{Z})$  for orthogonal  $\mathbf{Q}$
3. **Additivity:** For independent subspaces, effective dimensions approximately add
4. **Continuity:** Small perturbations in eigenvalues yield small changes in EffDim

These properties make effective dimension a robust measure for comparing representations across architectures with different nominal dimensions.

### 9.4 D. LLM Layer-wise Geometry Analysis

The decoder-only LLM analysis (Figure 8 in main text) reveals several key patterns:

- **Layer-wise progression:** Effective dimension typically increases through early layers then stabilizes or decreases in final layers
- **Family-specific signatures:** SmoLLM and Qwen models show consistently higher compression than GPT-2 family
- **Scale independence:** The correlation between compression and output effective dimension ( $r = 0.69$ ) is independent of model size ( $r = 0.07$  with hidden dimension)

### 9.5 E. Detailed Intervention Results

The causal intervention experiment (Figure 9 in main text) demonstrates direct manipulation of representation geometry using models with strong baselines (86-88% accuracy on CIFAR-10). Below we provide per-model statistics:

Model	Baseline Acc	Baseline Eff. Dim	Max ΔEffDim	Max Δacc
ResNet18	86.8%	9.8	+219.0	-1.5pp
ResNet34	85.9%	9.2	+216.6	-1.7pp
DenseNet121	88.4%	10.0	+666.4	-75.7pp
<b>Pooled</b>	—	—	—	$r = -0.94$

Table 12: Per-model intervention statistics with strong baselines. Gaussian noise consistently increases effective dimension (degrades geometric structure), with pooled correlation  $r = -0.94$ ,  $p < 10^{-9}$  between effective dimension change and accuracy change. DenseNet121 shows extreme sensitivity due to dense skip connections.

## 9.6 F. Training Dynamics: Additional Details

The training-time analysis (Figure 5 and Figure 6 in main text) tracks 11 models across 6 architecture families. Key observations:

- **Epoch 10:** Geometric metrics begin differentiating models, but correlations are weak ( $R^2 < 0.3$ )
- **Epoch 20:** Output effective dimension becomes significantly predictive of final accuracy
- **Epoch 30-50:** Both geometric metrics and early accuracy converge to strong predictive power ( $R^2 > 0.7$ )
- **Architecture consistency:** The pattern holds across ResNet, VGG, DenseNet, EfficientNet, MobileNet, and ShuffleNet families

The key insight is that geometric structure provides **earlier** signal about final performance than accuracy itself, making it valuable for model selection and early stopping decisions.

## 9.7 G. Bidirectional Intervention: Detailed Results

We test bidirectional causality by comparing geometry *degradation* (Gaussian noise) with geometry *improvement* (PCA projection) on ResNet18 (baseline: 86.84% accuracy, EffDim 9.8).

Intervention	Parameter	EffDim	ΔEffDim	ΔAccuracy
Baseline	—	9.8	—	86.84%
Noise $\sigma = 0.1$	degrade	13.3	+3.5	-0.11pp
Noise $\sigma = 0.2$	degrade	26.6	+16.8	-0.11pp
Noise $\sigma = 0.3$	degrade	55.9	+46.1	-0.47pp
Noise $\sigma = 0.4$	degrade	104.5	+94.7	-0.95pp
Noise $\sigma = 0.5$	degrade	166.6	+156.8	-0.93pp
PCA 99%	improve	9.6	-0.2	-0.03pp
PCA 95%	improve	8.8	-1.0	-0.02pp
PCA 90%	improve	8.1	-1.7	-0.05pp
PCA 80%	improve	7.4	-2.4	-3.02pp
PCA 70%	improve	6.5	-3.3	-5.18pp

Table 13: Complete bidirectional intervention results. **Degradation** (noise): increasing EffDim degrades accuracy ( $r = -0.92$ ,  $p = 0.026$ ). **Improvement** (PCA): decreasing EffDim maintains accuracy when sufficient variance is preserved. The asymmetry is informative: the network tolerates dimension *reduction* (PCA removes noise) better than dimension *inflation* (noise adds uninformative variance).

### Statistical analysis:

- Degradation correlation ( $\Delta$ EffDim vs  $\Delta$ Acc):  $r = -0.92$ ,  $p = 0.026$
- Improvement (PCA  $\geq 90\%$  variance): mean  $\Delta$ Acc =  $-0.03$ pp, demonstrating that accuracy is maintained when informative dimensions are preserved

**Interpretation:** The asymmetry between degradation and improvement is itself informative. Adding noise uniformly inflates all dimensions, corrupting task-relevant structure. PCA projection, by contrast, selectively removes low-variance dimensions that contribute little to classification. The fact that 9 components (out of 512) suffice for 86.79% accuracy reveals that the learned representation is highly structured—most variance lies in a small task-relevant subspace.

## 9.8 H. Multi-Noise Type Intervention: Detailed Results

To validate that the geometry-accuracy relationship is noise-type agnostic, we test four fundamentally different noise types on ResNet18 (baseline: 86.84% accuracy, EffDim 9.78). Each noise type has different statistical properties, allowing us to distinguish general geometric effects from noise-specific artifacts.

Noise Type	Param	EffDim	$\Delta$ EffDim	$\Delta$ Acc (pp)
Gaussian $\sigma$	0.1	13.3	+3.5	-0.13
	0.2	26.6	+16.8	-0.25
	0.3	56.1	+46.3	-0.49
	0.4	104.9	+95.2	-0.96
	0.5	165.3	+155.6	-0.98
Uniform $\pm$ range	0.1	10.9	+1.1	-0.15
	0.2	14.5	+4.8	-0.19
	0.3	21.7	+12.0	-0.21
	0.4	33.8	+24.1	-0.24
	0.5	51.7	+41.9	-0.43
Dropout rate	0.1	13.3	+3.5	-0.10
	0.2	18.4	+8.6	-0.42
	0.3	25.4	+15.6	-0.29
	0.4	35.8	+26.0	-0.79
	0.5	51.3	+41.5	-0.86
Salt-pepper rate	0.05	26.3	+16.6	-0.21
	0.10	54.0	+44.2	-0.41
	0.15	93.2	+83.4	-0.82
	0.20	142.0	+132.2	-1.08
	0.25	199.0	+189.2	-1.40

Table 14: Complete multi-noise intervention results. All noise types show consistent pattern: increasing noise  $\rightarrow$  increasing EffDim  $\rightarrow$  decreasing accuracy. Salt-and-pepper noise has the most dramatic effect on geometry (EffDim increases to 199 at 25% rate), while Gaussian noise produces the smoothest degradation curve.

### Statistical summary:

- Gaussian:  $r = -0.94, p = 0.016$
- Uniform:  $r = -0.96, p = 0.010$
- Dropout:  $r = -0.91, p = 0.033$
- Salt-pepper:  $r = -0.99, p = 0.001$
- **Pooled:**  $r = -0.91, p = 4.2 \times 10^{-8}$

All noise types show strong negative correlation despite fundamentally different perturbation mechanisms: Gaussian adds continuous noise, Uniform adds bounded noise, Dropout randomly zeros activations, and Salt-pepper sets random values to extremes. This universality validates that the geometry-accuracy relationship reflects fundamental representation properties.

## 9.9 I. Multi-Architecture PCA: Detailed Results

To verify that PCA intervention generalizes across architectures, we apply the same protocol to ResNet18, ResNet34, and DenseNet121. All models are trained on CIFAR-10 with strong baselines (86-88% accuracy).

Model	Var %	Comp.	EffDim	$\Delta$ EffDim	$\Delta$ Acc (pp)
ResNet18 (baseline 86.84%)	99%	48	9.58	-0.20	-0.02
	95%	16	8.81	-0.97	-0.04
	90%	9	8.09	-1.69	-0.15
	85%	8	7.37	-2.40	-2.79
	80%	8	7.37	-2.40	-2.79
ResNet34 (baseline 85.90%)	99%	44	9.04	-0.19	+0.02
	95%	14	8.34	-0.89	-0.06
	90%	9	7.83	-1.40	-0.02
	85%	8	7.17	-2.06	-2.08
	80%	8	7.17	-2.06	-2.08
DenseNet121 (baseline 88.37%)	99%	34	9.79	-0.20	-0.09
	95%	15	9.12	-0.86	+0.02
	90%	9	8.27	-1.72	+0.03
	85%	9	8.27	-1.72	+0.03
	80%	8	7.50	-2.48	-3.24

Table 15: Complete multi-architecture PCA results. All three architectures maintain accuracy at 90-99% variance thresholds with only 9-48 components. DenseNet121 shows slight accuracy *improvement* at 90-95% variance, suggesting PCA removes noise that disrupts dense connectivity. Accuracy degrades sharply below 85% variance threshold.

#### Cross-architecture summary at 95% variance:

- ResNet18: 16 components,  $\Delta$ acc = -0.04pp
- ResNet34: 14 components,  $\Delta$ acc = -0.06pp
- DenseNet121: 15 components,  $\Delta$ acc = +0.02pp
- **Mean:** 15 components,  **$\Delta$ acc = -0.03pp**

The consistent finding across architectures is that 15 principal components (out of 512) suffice to preserve task-relevant information. This validates that learned representations concentrate information in a low-dimensional subspace regardless of architectural family, and that this property can be exploited for dimensionality reduction without accuracy loss.